

## Structured catalyst for the catalytic combustion of soot: Co,Ba,K/ZrO<sub>2</sub> supported on Al<sub>2</sub>O<sub>3</sub> foam

E.D. Banús, V.G. Milt, E.E. Miró, M.A. Ulla \*

Instituto de Investigaciones en Catálisis y Petroquímica, INCAPE (FIQ, UNL-CONICET), Santiago del Estero 2829, 3000 Santa Fe, Argentina

### ARTICLE INFO

#### Article history:

Received 11 February 2009

Received in revised form 13 April 2009

Accepted 18 April 2009

Available online 24 April 2009

#### Keywords:

Structured catalyst

Soot combustion

Al<sub>2</sub>O<sub>3</sub> foam

ZrO<sub>2</sub> coating

### ABSTRACT

An alumina foam has been coated with a thin layer of ZrO<sub>2</sub> by washcoating and impregnated with Co, Ba and K, which are active ingredients for soot combustion and NO<sub>x</sub> adsorption processes. The ZrO<sub>2</sub> coating exhibits an arrangement of interconnected surface cracks, due to the shrinkage of the Zr(OH)<sub>x</sub> layer during the drying process, and the high temperature treatment (700 °C), needed to remove and burn the colloidal stabilizer present in the slurry used during the washcoating procedure. However, the coating showed a good adherence when subjected to an ultrasonic test, and improved after the impregnation of the active components (K, Ba and Co), probably due to a partial melting of the potassium salt. The ZrO<sub>2</sub>-foam was less active for the soot combustion compared to the Co,Ba,K/ZrO<sub>2</sub>-foam, confirming that the Co, Ba and K species present on the coating acted as active elements; thus, the process employed to incorporate them proved to be effective. Although a shrinkage–crack pattern of flakes (mainly composed of Co,Ba,K/ZrO<sub>2</sub>) and cracks (rich in Al<sub>2</sub>O<sub>3</sub>) was observed in the catalytic film, the system showed to be active and stable for the catalytic combustion of soot. The maximum in the combustion rate depends upon the amount of soot loaded and the presence of NO in the feed, having a performance comparable to that obtained with the powder catalyst.

© 2009 Elsevier B.V. All rights reserved.

### 1. Introduction

During the last decade, diesel engines have increased in popularity because of their superior fuel economy and durability. However, some aspects of the pollutant control of exhaust gases remain unsolved. Particulate matter (soot) and NO<sub>x</sub> are the diesel pollutants of major concern, the combination of a filter with oxidation catalysts being the most studied after-treatment process to eliminate soot particles. For NO<sub>x</sub> abatement, NO<sub>x</sub> adsorbers (traps) and NO<sub>x</sub> SCR with ammonia or hydrocarbons constitute novel technologies both for partial lean-burn gasoline engines and for diesel ones. The adsorber (usually containing Ba or K compounds) chemically binds nitrogen oxide during lean engine operation. After the adsorber capacity is saturated, the system is regenerated and released NO<sub>x</sub> is reduced during a period of rich operation. In the case of diesel engines, since a rich operation is not feasible, periodic fuel injections are necessary.

On the other hand, a large number of catalyst formulations have been reported for soot combustion, and the soot-to-catalyst contact appears to be one of the most important problems to overcome [1]. Interesting review articles on these subjects have

been published, dealing with filters for particulate diesel emission control [2,3], NO<sub>x</sub> abatement using sorbing catalytic materials [4] and fundamentals of oxidation carbon by NO<sub>x</sub> [5]. Some reviews [6–8] have recently offered updates on new technologies for diesel emission control. Despite the abundant studies on both soot combustion and NO<sub>x</sub> abatement carried out with powder formulations, not so many papers have been published using structured catalysts, which constitutes a more realistic approach.

In particular, for soot particles abatement, an adequate morphology of the catalyst is required so as to improve the contact between catalyst and soot. For practical purposes, the catalytically active component ought to be supported as a film on a structured substrate, thus allowing simultaneous soot filtration and combustion [9]. Among the various filter types (mainly monoliths, foams and yarns) [6], ceramic foams are attractive structured systems that can be prepared from a range of materials and have characteristics that make them desirable as substrates for structured heterogeneous catalysts [10]. They exhibit high porosities with a significant degree of interconnectivity among spherical-like cells through openings or windows, which results in low pressure drop [11]. While the more conventional wall-flow type monoliths act as “cake filters”, foams act as deep bed filters. These systems operate through different mechanisms: in the monoliths, the surface filtration gives good particulate collection efficiency, but a significant drop pressure occurs as the layer of soot

\* Corresponding author. Tel.: +54 342 4536861; fax: +54 342 4536861.  
E-mail address: [mulla@fiq.unl.edu.ar](mailto:mulla@fiq.unl.edu.ar) (M.A. Ulla).

particulates deposited on the filter walls grows. In the case of the deep filtration type filters (foams), a good penetration/dispersion of particulate inside the trap matrix is obtained [9], thus allowing constant collection efficiency. Although the retention efficiency is often low [2], this can be overcome with an appropriate trap design [12]. The use of different types of foams has been the object of several interesting research work aimed to eliminate diesel contaminants produced either by diesel cars or by gas–oil burners [9,12–25] and of other catalytic applications, such as CO<sub>2</sub> reforming [11]. By far, the most studied ceramic foams have been the Al<sub>2</sub>O<sub>3</sub> ones [9,10,12,14–17,22].

The catalytic film should be highly active for soot combustion, resistant to both thermal and mechanical shocks, and also resistant to poisons [26]. In this vein, Biamino et al. [27] developed a method for the deposition of catalysts on ceramic substrates, consisting in using impregnation techniques coupled with a combustion synthesis process to produce a well-adherent layer of perovskite catalyst directly on a ceramic honeycomb. Fino et al. [21] reported that a catalytic trap constituted by a ceramic foam covered with 13 wt.% Cs<sub>2</sub>O·V<sub>2</sub>O<sub>5</sub> catalyst results in an efficient and functional system for particulate elimination, but unfortunately, its performance is satisfactory only at about 400 °C, which limits its applicability to the treatment of stationary industrial sources. Ciambelli et al. found that alumina foam traps modified with Cu/V/K/Cl catalyst are efficient for soot filtration and combustion [14,17].

The above-described systems consist of the deposition of the catalytic film directly over the bare structured substrate. Nevertheless, a low surface area ceramic substrate gives desirable physical and mechanical properties but the choice of an adequate washcoat provides a high surface area [10] so that catalytic films could enhance their activities when depositing them on the washcoat-structured substrate. Besides, the washcoat avoids reactions between the catalytic components and the Al<sub>2</sub>O<sub>3</sub> substrate, which constitutes a frequent failure that affects the structured catalyst durability.

In this work, we present a promising system based on a Co,Ba,K/ZrO<sub>2</sub> catalyst deposited on an alumina foam to be used for the abatement of soot and NO<sub>x</sub> in diesel exhausts. We selected Co as active catalyst for soot combustion, K to improve the soot–catalyst contact, and Ba as a NO<sub>x</sub> trap. In a previous work, we demonstrated the efficiency of these ingredients for the simultaneous abatement of NO<sub>x</sub> and soot [28,29]. We selected ZrO<sub>2</sub> to generate a porous layer (washcoat) on which the active ingredients were deposited. The structured catalyst was evaluated for soot combustion and the adherence of the films was confirmed by means of an ultrasound test. The catalysts were characterized by XRD, FTIR, EDX and SEM in order to correlate the catalytic results with the physical-chemistry properties of the solids.

## 2. Experimental

### 2.1. Co,Ba,K deposited onto ZrO<sub>2</sub>-coated $\alpha$ -Al<sub>2</sub>O<sub>3</sub> foam: preparation

The  $\alpha$ -Al<sub>2</sub>O<sub>3</sub> foam (91% porosity and 65 ppi, Gimex) was used as substrate. Ciambelli et al. [14,17] reported that this kind of foam has a good efficiency to act as soot filter.

The structured catalyst was prepared in two stages: first, the deposition of a ZrO<sub>2</sub> layer over the foam (ZrO<sub>2</sub>-foam) and second, the deposition of the active metals (Co,Ba,K/ZrO<sub>2</sub>-foam). ZrO<sub>2</sub> was added in order to both increase the specific surface area and avoid metal–support interactions between the active components and the support.

The ZrO<sub>2</sub> coating was deposited onto  $\alpha$ -Al<sub>2</sub>O<sub>3</sub> foam from a colloidal ZrO<sub>2</sub> suspension (Nyacol, 20 wt.%, acetate stabilized, particle size 5–10 nm) by washcoating (immersion time = 1 min).

Then, it was softly blown and dried at 130 °C for 12 h in a stove after which it was calcined at 700 °C for 2 h in air. In the second stage, the active components (Ba, Co and K) were deposited using an impregnation solution containing Ba(Ac)<sub>2</sub>, Co(Ac)<sub>2</sub> and KNO<sub>3</sub>, where the atomic metal percentages were K: 35.9%, Co: 40.7% and Ba: 23.4%, and the Ba(Ac)<sub>2</sub> concentration was 0.05 M. These ratios had been chosen to be the same as those used in the preparation of the powder (not structured) catalyst [29]. After the immersion during 1 min of the ZrO<sub>2</sub>-containing foam into the Co, Ba and K solution, the system was softly blown and dried at 130 °C for 12 h and then it was calcined at 500 °C in air for 2 h.

### 2.2. Characterization

#### 2.2.1. X-ray diffraction (XRD)

The X-ray diffractograms were obtained with a Shimadzu XD-D1 instrument with monochromator using Cu K $\alpha$  radiation at a scan rate of 1°/min, from 2 $\theta$  = 10° to 70°, after crushing the samples in an agate mortar. The software package of the equipment was used for the phase identification.

#### 2.2.2. IR spectroscopy (FTIR)

Infrared spectra were obtained using a Shimadzu IR Prestige-21 spectrometer. The samples were crushed in an agate mortar and then prepared in the form of pressed wafers (ca. 1% sample in KBr). All spectra involved the accumulation of 80 scans at 4 cm<sup>-1</sup> resolution.

#### 2.2.3. Scanning electron microscope (SEM)

A SEM Jeol JSM-35C equipment was employed operated at 20 kV acceleration voltage. Samples were glued to the sample holder with Ag painting and then coated with a thin layer of Au in order to improve the images.

#### 2.2.4. Energy-dispersive X-ray spectroscopy (EDX)

The elemental chemical analysis was performed trying the X-ray spectra with the EDAX software. Semi quantitative results were obtained with the theoretical quantitative method (SEMIQ), which does not require standards. X-ray spectra were obtained with an acceleration of 20 kV.

#### 2.2.5. Adherence test

A Testlab TB04 equipment was used to measure the weight loss caused when exposing the sample to an ultrasound bath. The samples were immersed into either acetone or water and subjected to ultrasound at 25 °C, varying the treatment time among 1 and 30 min.

### 2.3. Catalytic soot combustion

The soot was obtained by burning commercial diesel fuel (Repsol – YPF, Argentina) in a glass vessel. After being collected from the vessel walls, the soot was dried in a stove at 120 °C for 24 h. More details about the obtention and characterization of soot are reported elsewhere [30].

The soot was dispersed in *n*-hexane using an ultrasonic bath for its good dispersion. In order to vary the soot/catalyst ratio, dispersions of different concentrations (600, 1500 and 6000 ppm) were prepared to impregnate by dipping either the structured catalyst (Co,Ba,K/ZrO<sub>2</sub>-foam) or the structured support (ZrO<sub>2</sub>-foam) during 1 min. Then, they were dried at room temperature.

The effect of the solvent used for the preparation of the soot suspension was also studied. For this purpose, a comparison between a polar solvent (H<sub>2</sub>O) and a non-polar solvent (*n*-hexane) was performed and the SEM technique was employed to analyze the contact between the soot and the structured catalyst.

The activity of the structured catalyst and structured support for the soot combustion was studied by temperature programmed oxidation (TPO). For this purpose the soot/catalyst mixtures were heated at 5 °C/min from room temperature up to 600 °C (structured catalyst) or 650 °C (structured support), in O<sub>2</sub> (18%) diluted in helium balance (total flow 20 ml/min) in a flow equipment designed for this purpose. The exhaust gases were analyzed with a Shimadzu GC-2014 chromatograph (with TCD detector), the CO concentration being negligible. This fact is due to the presence of cobalt oxide, which is a good catalyst for CO oxidation, and this is in agreement with previously reported results [31].

Considering the coating weight gains and that all the soot added to the structured catalyst was burned during the TPO experiment, it was possible to estimate the Co,Ba,K/ZrO<sub>2</sub> coating–soot ratio. The average ratios obtained of using soot suspensions of 600, 1500 and 6000 ppm in hexane were 6, 4, and 2, respectively.

The effect of the presence of 0.1% NO was studied by feeding O<sub>2</sub> (18%) + NO (0.1%) diluted in helium (total flow 20 ml/min) and carrying out the catalytic tests as previously described, heating the soot/catalyst mixtures at 5 °C/min from room temperature up to 600 °C (catalyst supported on the foam) or 650 °C (only the foam).

The repetitivity of the activity measurements was assessed by the following procedure: (i) impregnating an aliquot of the structured catalyst (or the structured support) with soot using the suspension of 600 ppm in *n*-hexane, (ii) carrying out the TPO experiment, (iii) extracting the structured system after the burning of soot; and (iv) starting all over again from (i). A curve of produced CO<sub>2</sub> versus temperature was then obtained, where the area under the peaks is directly proportional to produced CO<sub>2</sub>, i.e., to the soot loaded in the structured catalyst.

The carbon conversions at different reaction temperatures, using 0.1% of NO, were calculated for the three coating–soot ratios obtained. This calculation was done as described in reference [29]. For comparison, the carbon conversion profile of the Co,Ba,K/ZrO<sub>2</sub> powder catalyst, using a tight contact with a catalyst–soot ratio: 6 was also determined.

### 3. Results

#### 3.1. Co,Ba,K/ZrO<sub>2</sub> coating preparation

After coating the original foam with colloidal ZrO<sub>2</sub> and drying at 130 °C, the weight gaining percentage was around 16 wt.% (Fig. 1). But after calcination at 700 °C, the sample lost weight because of the adsorbed water removal and the colloidal ZrO<sub>2</sub> stabilizing agent (acetic acid) combustion, so that the final weight gaining percentage was about 10 wt.%. A good reproducibility of the coating process was achieved as it is shown for the three different batches (Fig. 1 and Table 1).

For the incorporation of the active components, Co, Ba and K (second stage), 10 cycles of immersion–blowing–drying–calcination were carried out. For each cycle, the weight gaining percentage was almost the same; consequently this percentage

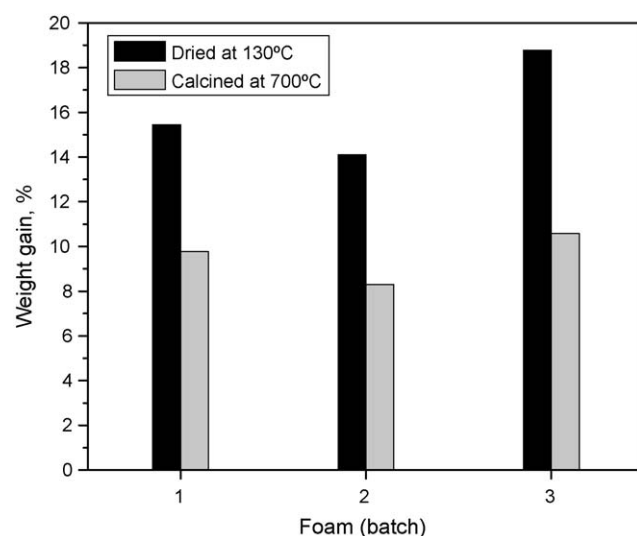


Fig. 1. Weight gain percentage after coating the original  $\alpha$ -Al<sub>2</sub>O<sub>3</sub> foam with colloidal ZrO<sub>2</sub> for three different aliquots: (a) dried at 130 °C and (b) calcined at 700 °C.

increased linearly with the number of cycles, after 10 cycles being nearly 5 wt.% (Fig. 2).

#### 3.2. Crystalline phases and components present in the Co,Ba,K/ZrO<sub>2</sub>-foam

The XRD results shown in Fig. 3 indicate that the original foam contains  $\alpha$ -Al<sub>2</sub>O<sub>3</sub> as the main crystalline phase and that aluminosilicates (Al<sub>2</sub>SiO<sub>5</sub> and Al<sub>6</sub>Si<sub>2</sub>O<sub>13</sub>) are also present as impurities (Fig. 3a). Besides, the presence of the  $\theta$ -phase of Al<sub>2</sub>O<sub>3</sub> at trace level cannot be discarded. When the foam was coated with a layer of ZrO<sub>2</sub>, both the monoclinic and the tetragonal structures of ZrO<sub>2</sub> are observed, in addition to the  $\alpha$ -Al<sub>2</sub>O<sub>3</sub> signals (Fig. 3b). Note, nevertheless, that the aluminosilicate peaks disappear as the ZrO<sub>2</sub> coating is produced. This might be associated with reactions between the aluminosilicates and the ZrO<sub>2</sub> to give Al<sub>2</sub>O<sub>3</sub> plus a Si–Zr compound, like a solid solution.

The fraction of the monoclinic ZrO<sub>2</sub> phase ( $x_m$ ) was estimated as 0.60 using the integrated peak intensity of the [1 0 1] plane of the tetragonal phase ( $I_{t[101]}$ ) and the [1 1 1] and  $[\bar{1} 1 1]$  planes of the monoclinic phase ( $I_{m[111]}$  and  $I_{m[\bar{1}11]}$ ) and the following equation [32]:

$$x_m = 1 - \left[ \frac{I_{t[101]}}{(I_{t[101]} + I_{m[111]} + I_{m[\bar{1}11]})} \right]$$

In the XRD pattern of Co,Ba,K/ZrO<sub>2</sub>-foam catalyst (Fig. 3c), signals corresponding to BaCO<sub>3</sub> are observed, in addition to the  $\alpha$ -Al<sub>2</sub>O<sub>3</sub> and the monoclinic and tetragonal ZrO<sub>2</sub> phase peaks. Besides, the fraction of the monoclinic ZrO<sub>2</sub> phase remains almost the same: 0.57. Signals of neither K nor Co containing crystalline phases are observed.

Table 1

Weight changes during the preparation of the structured catalyst.

Preparation	Initial foam weight (g) (i)	Weight foam + washcoat ZrO <sub>2</sub> (ZrO <sub>2</sub> -foam), calcined at 700 °C (g) (ii)	Gained weight of ZrO <sub>2</sub> (%) <sup>a</sup>	Weight foam + washcoat ZrO <sub>2</sub> + cations (Co,Ba,K-ZrO <sub>2</sub> -foam), after calcination at 500 °C (g) (iii)	Weight percentage of cations <sup>b</sup>
1	0.2692	0.2955	9.77	0.3085	4.40
2	0.2530	0.2740	8.30	0.2864	4.53
3	0.1635	0.1808	10.58	<sup>c</sup>	<sup>c</sup>

<sup>a</sup> Weight percentage with respect to the foam  $((ii - i)/i) \times 100$ .

<sup>b</sup> Weight percentage with respect to the ZrO<sub>2</sub>-foam  $((iii - ii)/ii) \times 100$ .

<sup>c</sup> These values could not be measured because the structured system was broken during the cations deposition.

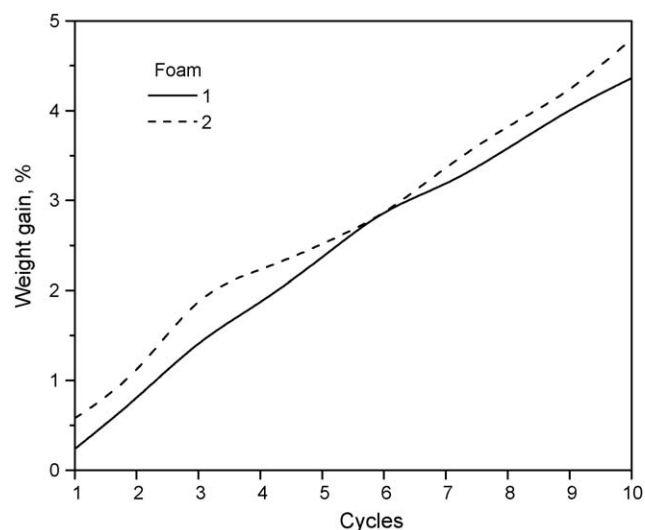


Fig. 2. Weight gain percentage after each cycle of active element incorporation: Co, Ba and K.

According to Miller [33], the IR spectrum of the bare foam, shown in Fig. 4a, is consistent with  $\text{Al}_2\text{O}_3$ . No significant differences between this IR spectrum and that of the  $\text{ZrO}_2$ -foam were observed (compare Fig. 4a and b), whereas the IR spectrum of the Co,Ba,K/

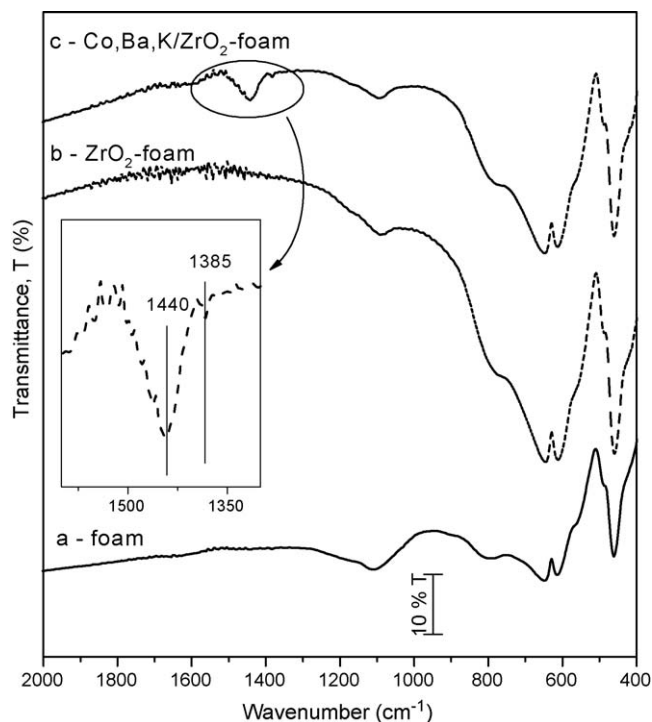


Fig. 4. FTIR spectra of (a) substrate:  $\alpha$ - $\text{Al}_2\text{O}_3$  foam, (b) structured support:  $\text{ZrO}_2$ -foam and (c) structured catalyst: Co,Ba,K/ $\text{ZrO}_2$ -foam.

$\text{ZrO}_2$ -foam catalyst (Fig. 4c) presents two new signals at 1440 and  $1385\text{ cm}^{-1}$ . The former is associated with carbonate species, which are attributed to the presence of the  $\text{BaCO}_3$  phase, in agreement with the XRD results (Fig. 3). The signal at  $1385\text{ cm}^{-1}$  corresponds to the  $\nu_{\text{NO}_3^-}$  stretching and is probably related to  $\text{KNO}_3$ , as it was the salt used during the catalyst preparation.

### 3.3. Morphology of Co,Ba,K/ $\text{ZrO}_2$ -foam

The SEM micrographs in Fig. 5 show the structure and surface morphology of the original  $\alpha$ - $\text{Al}_2\text{O}_3$  foam, which has an open-cell structure. The cells are approximately spherical voids enclosed by struts and windows; the latter are openings connecting the cells to each other (Fig. 5a). The cell surface is to a certain extent rough (Fig. 5b and c), having some macropores (Fig. 5d).

After immersing the  $\alpha$ - $\text{Al}_2\text{O}_3$  foam into the  $\text{ZrO}_2$  suspension, the substrates were calcined at two different temperatures: 500 or  $700\text{ }^\circ\text{C}$ . The morphology of the  $\text{ZrO}_2$  coatings obtained at these temperatures is shown in Fig. 6b and c in comparison to that of the  $\text{ZrO}_2$ -foam exposed at room temperature overnight (Fig. 6a). In general, all the coatings exhibit an arrangement of interconnected surface cracks, even the sample left at room temperature overnight and in this particular case, the structure is a mosaic-type one (Fig. 6a). However, for the  $\text{ZrO}_2$  coatings calcined at higher temperatures, the formation of flakes and wider cracks due to the shrinkage mechanism that occurs during the drying process is observed (Fig. 6b and c). After calcination at  $500\text{ }^\circ\text{C}$ , the coating color was black but changed to white as the treatment temperature increased to  $700\text{ }^\circ\text{C}$ , indicating that the latter temperature is needed to remove the residual carbon compounds.

Fig. 7 shows the morphology of the coating after the incorporation of the Co, Ba and K active elements. Even though the interconnected cracks with flake structure are still present in the coating (Fig. 7a and d), it is important to remark that the interaction between the flakes and the surface foam improves significantly as detected in the high magnification views of the sample (Fig. 7b and e). Cracks do not seem to propagate, indicating

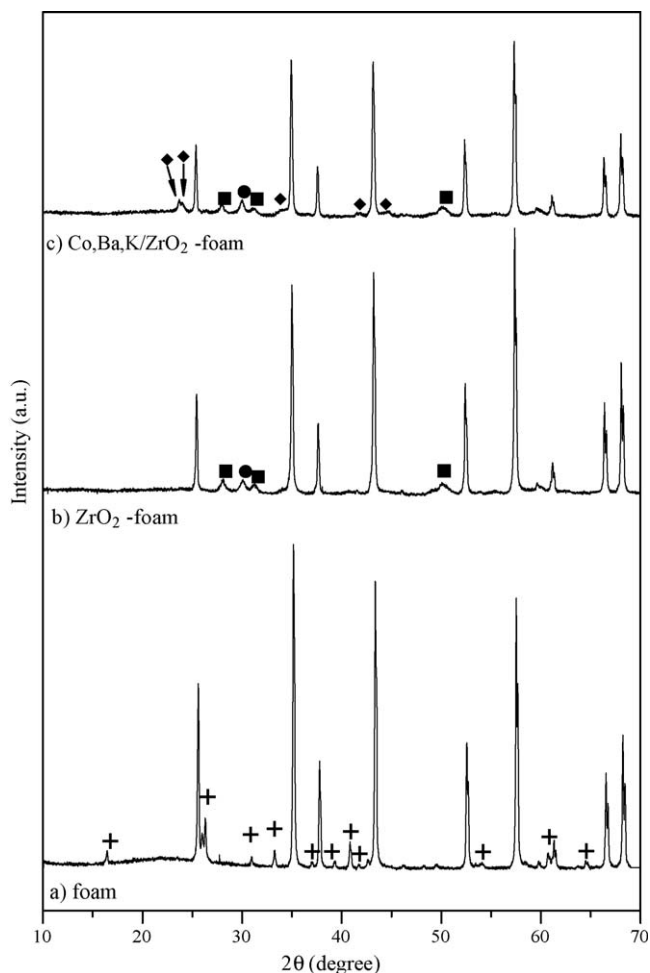


Fig. 3. Changes in the crystalline phases when adding the  $\text{ZrO}_2$  coating and the catalyst to the structured substrate ( $\alpha$ - $\text{Al}_2\text{O}_3$  foam) – ■:  $\text{ZrO}_2$  (monoclinic), ●:  $\text{ZrO}_2$  (tetragonal), ◆:  $\text{BaCO}_3$  and +: aluminosilicates ( $\text{Al}_2\text{SiO}_5$  and  $\text{Al}_6\text{Si}_2\text{O}_{13}$ ).  $\alpha$ - $\text{Al}_2\text{O}_3$  peaks (support) are not denoted.

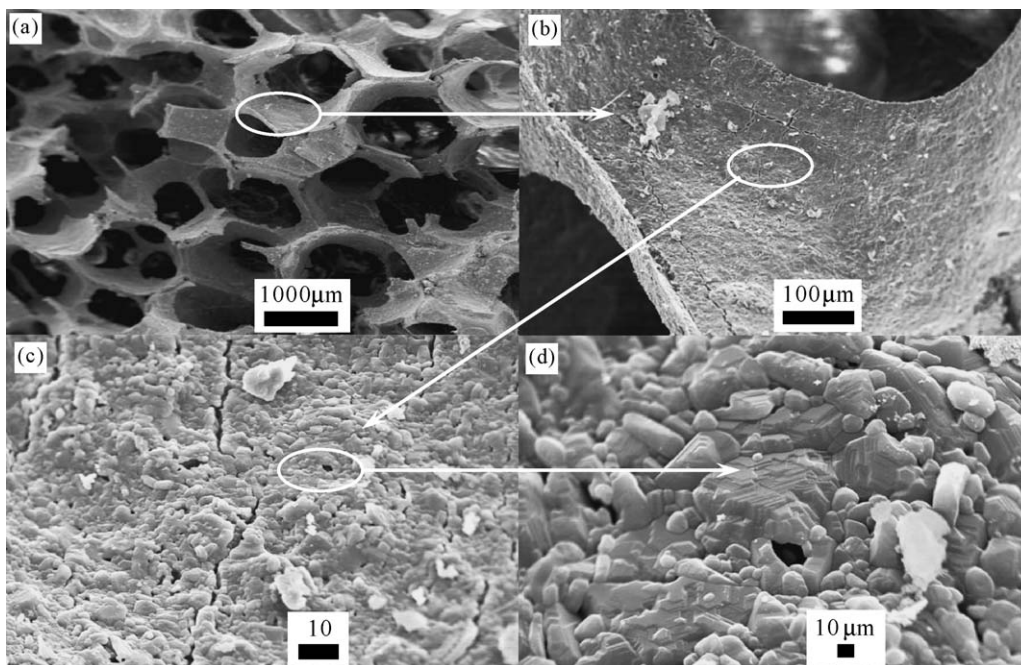


Fig. 5. SEM micrographs of the  $\alpha$ - $\text{Al}_2\text{O}_3$  foam without any additional treatment. Magnification: (a)  $\times 20$ , (b)  $\times 180$ , (c)  $\times 1000$  and (d)  $\times 4000$ .

strong adhesion of the coating to the substrate [34]. In addition, a close examination of the flake surfaces (Fig. 7c and f) points out some differences in morphology among them, which might be caused by different solvent evaporation rates. Note the bigger size of the flakes formed after the Co, Ba and K addition when comparing with the  $\text{ZrO}_2$ -foam system (Figs. 6c and 7b and e).

The Zr/Al and the  $M/(Zr + Al)$  ratios (M: Co, Ba or K) were estimated using EDX at two different regions of the Co,Ba,K/ $\text{ZrO}_2$  coating: flakes and cracks (Tables 2 and 3). The Zr/Al ratio indicates that Zr is mostly concentrated in the flakes, whereas in the cracks its concentration is too low (compare the first column of both Table 2 and Table 3). Concerning the active elements, Co, Ba and K,

their loadings are significantly higher over flakes than over cracks (compare Tables 2 and 3). However, in average, the atomic composition among them is quite similar for both regions (Table 4). This indicates that Co, Ba and K deposit mainly on flakes than on cracks, but whatever the deposited amount, the relative concentration of metals (Co, Ba and K) is almost the same.

### 3.4. Coating adhesion

To check the adherence of the  $\text{ZrO}_2$  and the Co,Ba,K/ $\text{ZrO}_2$  coatings, the samples were submitted to an ultrasonic bath. Valentini et al. [35] have recently applied this kind of analysis for

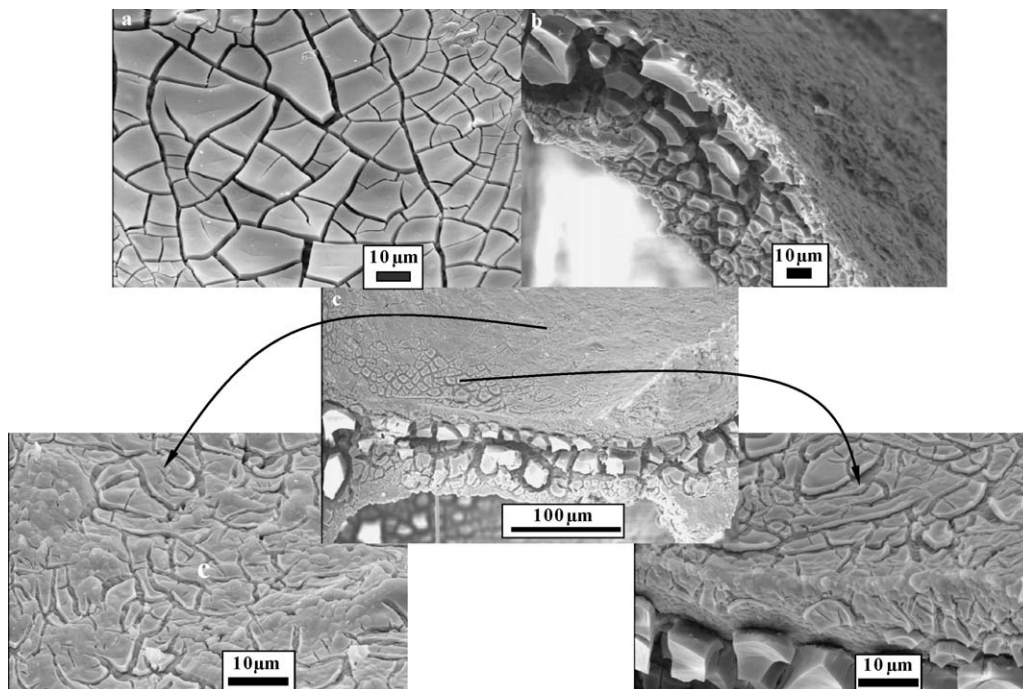


Fig. 6. SEM micrographs of the  $\text{ZrO}_2$ -foam after: (a) drying at  $25^\circ\text{C}$ , (b) calcination at  $500^\circ\text{C}$  and (c) calcination at  $700^\circ\text{C}$ .

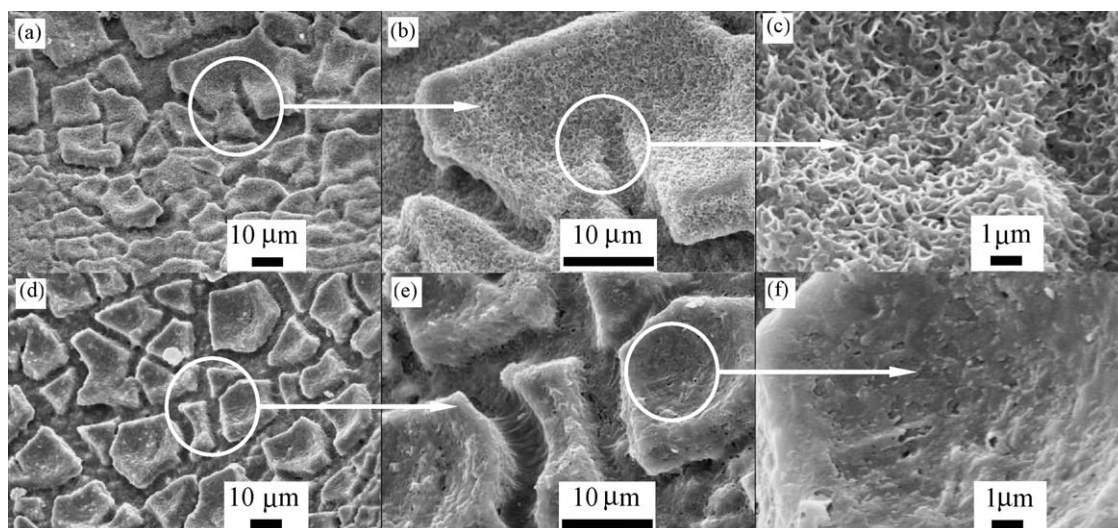


Fig. 7. SEM micrographs of Co,Ba,K/ZrO<sub>2</sub>-foam with three different magnifications: (a and d)  $\times 1000$ , (b and e)  $\times 3000$  and (c and f)  $\times 10,000$ .

alumina layers on ceramic and metallic supports and by Beers et al. [36] and Zamaro et al. [37] for checking adherence of in situ zeolite growth on monoliths.

In our analysis, acetone was used because it is a non-polar solvent, which avoids the dissolution of the active components (soluble in polar solvents as water or ethanol). If the dissolution occurs, the weight loss is not only due to the loss of deposited material (Co,Ba,K/ZrO<sub>2</sub>) onto the foam, but also because of the dissolution of the active components. Results of the stability of the ZrO<sub>2</sub> and the Co,Ba,K/ZrO<sub>2</sub> layer are observed in Fig. 8, where it can be seen that after 90 min of treatment, there was only 1.19 wt.% loss in the mass of the structured catalyst. However, it is worth noticing that this weight loss is observed at the beginning of the ultrasonic treatment (during the first 10 min) and after this period, the weight of the structured catalyst remains constant. In the case of the ZrO<sub>2</sub>-foam, the weight loss was slightly higher (1.5 wt.%) than in the case of the Co,Ba,K/ZrO<sub>2</sub>-foam (Fig. 8), which could be

associated with the difference in morphology observed in Figs. 6 and 7.

### 3.5. Catalytic soot combustion

The soot incorporation to the samples was done by their immersions in a soot suspension. Two solvents were used to prepare this suspension: water (polar solvent) and *n*-hexane (non-polar solvent). SEM micrographs show that the soot particles were better dispersed in the non-polar solvent, *n*-hexane (Fig. 9a and b) than in the polar one, water (Fig. 9c and d), thus producing smaller soot aggregates and a better contact between the dispersed soot and the structured catalyst. Also, the solubility of the active components in *n*-hexane is negligible, thus avoiding the loss of catalytic material. Moreover, van Setten et al. [38] studied two techniques for adding the soot on the catalytic foam: via either impregnation from soot dispersed in heptane, or by filtering soot derived from an aerosol. They sustain that they are equivalent techniques yielding similar coating–soot contact, which in turn are related to the soot oxidation rate. For these reasons, the non-polar solvent was chosen for the preparation of the soot dispersions. Nevertheless, it should be pointed out that the soot–catalyst contact is considered “loose” under these conditions [1].

Table 2

Co,Ba,K/ZrO<sub>2</sub>-foam: elemental atomic ratios on different flake regions.

Zr/Al	K/(Zr + Al)	Co/(Zr + Al)	Ba/(Zr + Al)
11.6	0.11	0.58	0.66
11.4	0.06	0.22	0.06
13.0	0.10	0.88	0.36
$\infty$	0.06	0.30	0.10

Table 3

Co,Ba,K/ZrO<sub>2</sub>-foam: Elemental atomic ratios on different crack regions.

Zr/Al	K/(Zr + Al)	Co/(Zr + Al)	Ba/(Zr + Al)
0.01	0.01	0.10	0.04
0.01	0.01	0.08	0.01
0.03	0.01	0.06	0.01
0.02	0.01	0.08	0.01
0.08	0.01	0.10	0.02

Table 4

Average atomic percentage of the active elements, Co, Ba and K, on different coating regions in comparison to those of the original impregnation solution.

Region	K (at.%)	Co (at.%)	Ba (at.%)
Flakes	7.7 (s.d. 2.6)	68.9 (s.d. 4.0)	23.4 (s.d. 4.7)
Cracks	8.4 (s.d. 2.5)	67.7 (s.d. 6.4)	23.9 (s.d. 7.5)
Impregnation solution	35.9	40.7	23.4

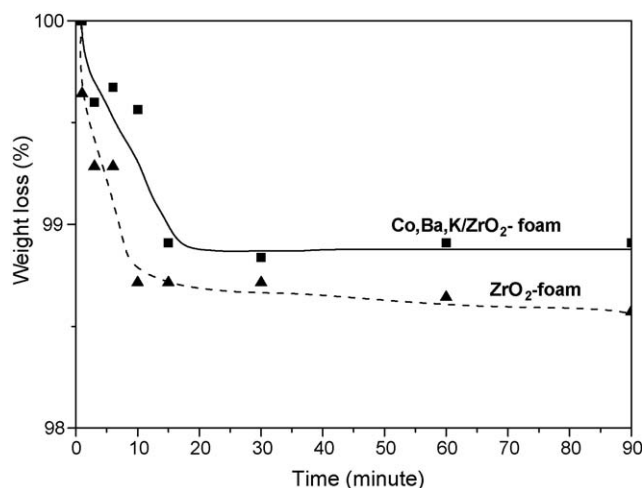


Fig. 8. Stability test (ultrasonic bath with acetone) of the structured system: - Co,Ba,K/ZrO<sub>2</sub>-foam and -ZrO<sub>2</sub>-foam.

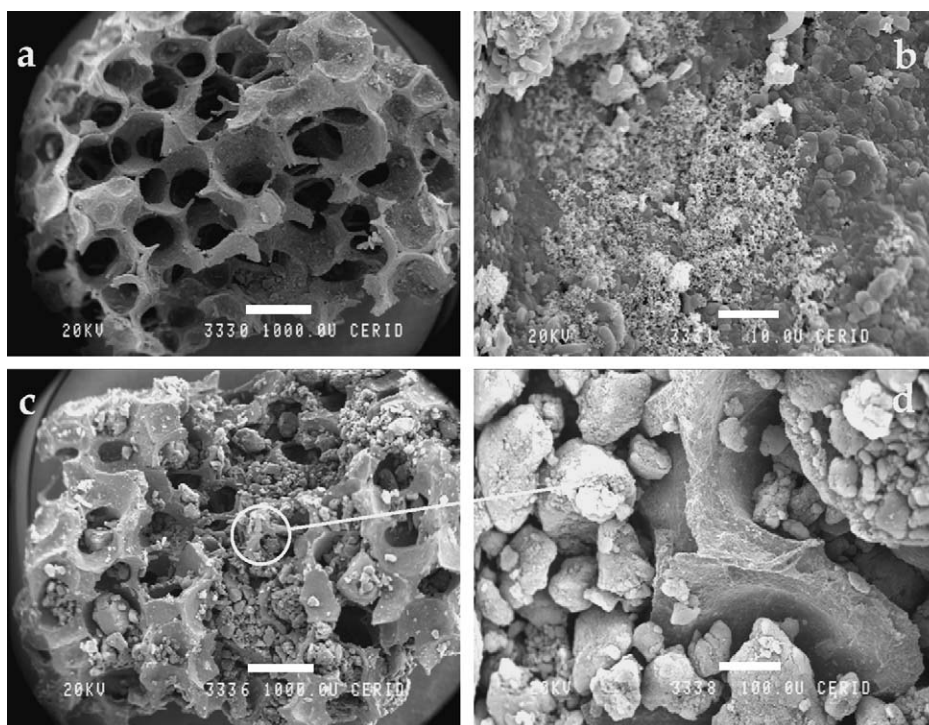


Fig. 9. Addition of soot particles via a soot suspension in: (a and b) *n*-hexane and (c and d) H<sub>2</sub>O.

Fig. 10 also shows the effect of the soot loading when the Co,Ba,K/ZrO<sub>2</sub>-foam and ZrO<sub>2</sub>-foam were impregnated with different soot concentrations. As expected, the temperature of maximum combustion rate shifted to higher values as the amount of soot increased. For the structured catalyst, the temperature of maximum combustion rate (maximum CO<sub>2</sub> concentration) was 420 °C using a suspension of 6000 ppm of soot in *n*-hexane (Fig. 10a). However, the temperature of this maximum decreased close to 370 °C when the impregnation was performed with the other two soot concentrations, 1500 and 600. This value is ca. 100 °C, less than that corresponding to the structured support (ZrO<sub>2</sub>-foam), which was near 450 °C (Fig. 10b). These results confirm that the Co, Ba and K species present on the coating acted as active elements for the soot combustion. Thus, the process used to incorporate them proved to be effective.

Fig. 11 shows that the catalytic test is considerably repetitive, the temperature of maximum combustion rate varying less than 4% both in the case of the structured catalyst (Fig. 11a) and in the case of the structured support (Fig. 11b), being  $383.8 \pm 13.8$  °C for the Co,Ba,K/ZrO<sub>2</sub>-foam and  $456.7 \pm 6.7$  °C for the ZrO<sub>2</sub>-foam.

The effect of the addition of NO in the feed was also studied. It is known that NO in presence of oxygen forms NO<sub>2</sub>, which is a better oxidant than O<sub>2</sub>. These results are shown in Fig. 12, where it can be observed that whatever the amount of loaded soot, the temperature of maximum combustion rate is always lower when NO is present in the feed.

The carbon conversion profiles using 0.1% of NO for the three coating-soot ratios obtained are shown in Fig. 13. These profiles indicate that the coating-soot ratios 6 and 4 have an analogous catalytic performance. In addition, the carbon conversion curve of coating-soot ratio: 6 is compared with that of the powder catalyst, Co,Ba,K/ZrO<sub>2</sub> using a tight catalyst-soot mixture with a ratio of 6 (Fig. 14). At low carbon conversion, powder and structured catalysts present comparable behavior. More complete kinetic models able to simulate TPO profiles are being developed [39].

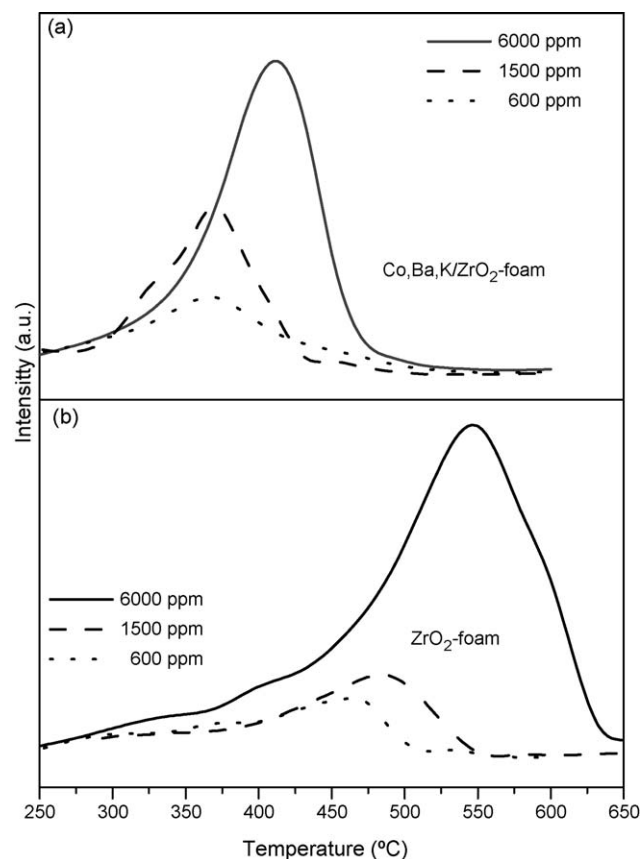
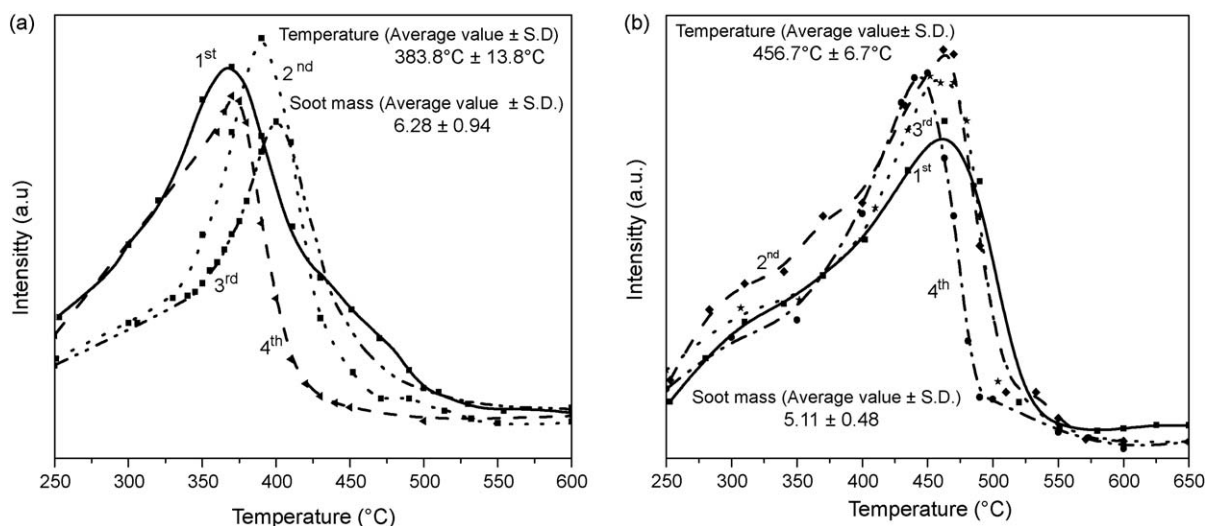
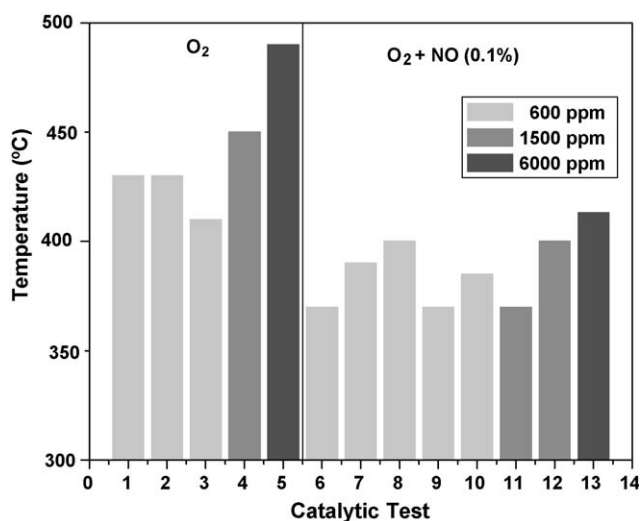


Fig. 10. Comparison between the activities of the structured catalyst (Co,Ba,K/ZrO<sub>2</sub>-foam) and the structured support (ZrO<sub>2</sub>-foam) on the soot combustion rate. Feed: total flow 20 ml/min (18% O<sub>2</sub>, 0.1% NO, He balance).



**Fig. 11.** Repetitivity of the catalytic measurements: (a) Co,Ba,K/ZrO<sub>2</sub>-foam and (b) ZrO<sub>2</sub>-foam. Feed: total flow 20 ml/min (18% O<sub>2</sub>, 0.1% NO, He balance). Soot loaded from a suspension of 600 ppm in *n*-hexane.



**Fig. 12.** Effect of the presence of NO in the temperature of maximum combustion rate. Feed: total flow 20 ml/min (18% O<sub>2</sub>, 0.1% NO, He balance).

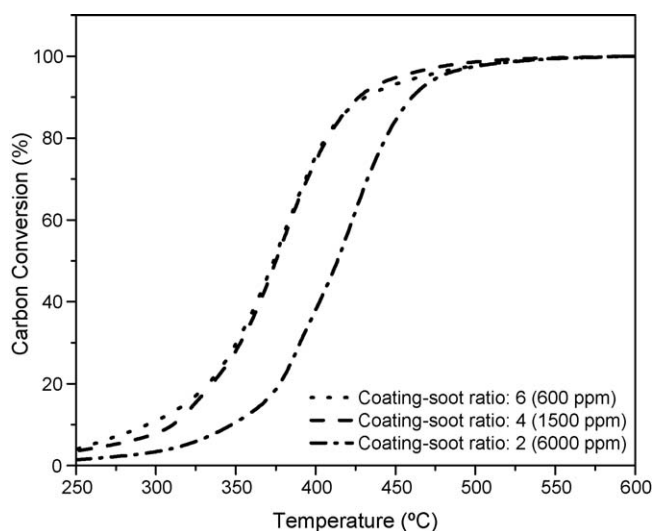


**Fig. 13.** The carbon conversion profile of Co,Ba,K/ZrO<sub>2</sub>-foam for the three coating-soot ratios: 6, 4 and 2. Feed: total flow 20 ml/min (18% O<sub>2</sub>, 0.1% NO, He balance).

## 4. Discussion

### 4.1. Characteristics of the Co,Ba,K/ZrO<sub>2</sub> coating onto the Al<sub>2</sub>O<sub>3</sub> foam

After one immersion of the Al<sub>2</sub>O<sub>3</sub> foam into the colloidal ZrO<sub>2</sub> suspension and the following calcination at 700 °C, a flake and mosaic-like layer with interconnected cracks was obtained, whose thickness was approximately 8 μm. Flakes and mosaics were not homogeneously distributed: there were zones rich in flakes and others mainly composed by mosaics. The coating crystalline phases were monoclinic and tetragonal ZrO<sub>2</sub>. Despite the aspect of the coating (flake and mosaic-like structure), both the process reproducibility and the coating adherence were good, as indicated by Fig. 1 and the adhesion test (Fig. 8).

After the colloidal ZrO<sub>2</sub> layer deposition, the drying and the calcination steps were critical for the final coating morphology since several phenomena take place simultaneously [40]. First of all, the solvent removal, which involves a combination of mass and heat transfer processes, can influence the generation of cracks on the ZrO<sub>2</sub> layer. Besides, it is expected that the ZrO<sub>2</sub> nanoparticles in the colloidal suspension used be, in fact, hydrated particles:

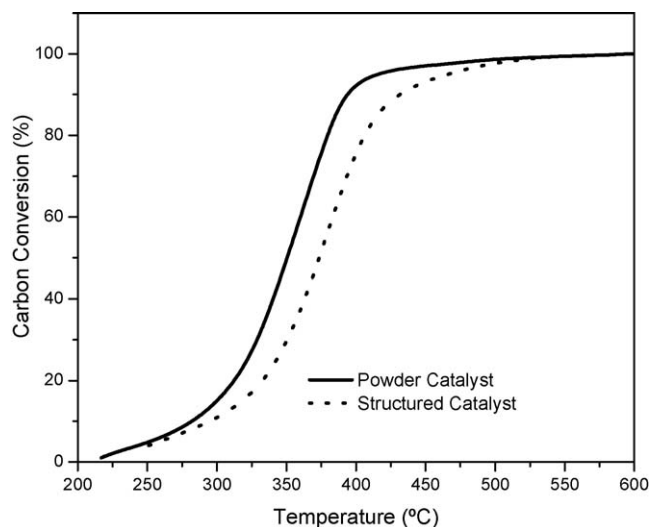


**Fig. 14.** Comparison of the carbon conversion profile between the structured catalyst (coating-soot ratio: 6) and the powder catalyst (catalyst-soot ratio: 6). Feed: total flow 20 ml/min (18% O<sub>2</sub>, 0.1% NO, He balance).

Zr(OH)<sub>x</sub> [41]. The IR spectrum (not shown) confirmed the hydrous nature of our ZrO<sub>2</sub> deposit. Therefore, the cracking in the coating can also be produced by the shrinkage of the hydrous films during the drying process, as reported for MoO<sub>x</sub> films [42]. The high temperatures needed to remove and burn the colloidal suspension stabilizer, acetic acid, can also contribute to the development of cracks, flakes and mosaics during the post-coating calcination step [43].

The incorporation of the active elements, Co, Ba and K, onto the ZrO<sub>2</sub>-foam, was done via 10 cycles of immersion into the cation-containing solution, followed by blowing, drying and calcining. The final weight gain percentage was about 4.5 wt.%. Although the coating morphology of the Co,Ba,K/ZrO<sub>2</sub>-foam presents similar characteristics to that of the ZrO<sub>2</sub>-foam (interconnected cracks, flakes and mosaics) (Fig. 7a and d), a closer view of the flakes reveals a significant improvement of their anchorage to the foam surface (Fig. 7b and c). Besides, the greater size of the flakes could probably be due to the combination of smaller flakes. This better coating adherence is confirmed with the adhesion test (Fig. 8), where the weight loss percentage was only 1.19 wt.%. Both evidences indicate that incorporating the active components in a second stage constitutes an advantage.

The presence of potassium in the immersing solution is another factor to be considered, since the low melting point of the potassium salt used in the preparation of the catalyst (KNO<sub>3</sub>) could help to the enhanced adherence of the coating.

According to the XRD pattern of the Co,Ba,K/ZrO<sub>2</sub>-foam catalyst, the catalytic layer contains mainly tetragonal and monoclinic ZrO<sub>2</sub>, the monoclinic fraction being quite similar to that of the ZrO<sub>2</sub>-foam. The contribution of several small peaks is also observed, which corresponds to BaCO<sub>3</sub>. This is in clear agreement with the IR results, where the presence of the NO<sub>3</sub><sup>-</sup> group, attributed to KNO<sub>3</sub>, is also observed. No signals associated with Co components are identified suggesting that the transition metal element is well dispersed on the surface layer.

The SEM-EDX technique is appropriate to analyze the distribution of the active elements on the different coating areas: cracks and flakes. It is important to remark that although results obtained using this technique are semi quantitative ones, for the sake of comparison, they gave us valuable information when trying to characterize these complex systems. Comparing the Co, Ba and K loadings over both areas (Tables 2 and 3) it is inferred that during the incorporation of the active components, the flake areas were able to retain higher amounts of the impregnation solution than the crack areas. This difference could be attributed to the fact that flakes (mainly composed of ZrO<sub>2</sub>) have pores whereas cracks (α-Al<sub>2</sub>O<sub>3</sub>) are almost non-porous. Therefore, the impregnation medium is sucked into the flake due to capillary force and remains in the pores after the blowing procedure, consequently retaining higher amounts of the active components at the end of each cycle.

It is noticeable that the distribution of the active elements, Co, Ba and K, on different flakes is not homogeneous (Table 2). The non-homogeneous compositions among them would be a consequence of the flake configurations since the concave surface may retain some solution after the blowing procedure. The microanalysis indicates a non-uniform deposition of the active components, which determines that the surface of the structured catalyst is not equally active.

Even though the Co, Ba and K contents differ between flakes and cracks, their atomic percentage compositions remain the same for both regions. In addition, the K atomic percentage is remarkably lower than that of the original impregnation solution (Table 4) suggesting that during the subsequent impregnation–blowing–drying–calcination cycles part of the alkaline component either might be re-dissolved or there might be a preferential adsorption

of Co on the ZrO<sub>2</sub>-foam surface. Besides, a loss of potassium during the calcination step is not discarded.

#### 4.2. Activity of the Co,Ba,K/ZrO<sub>2</sub>-foam system for the combustion of soot

The addition of soot particles to the structured catalyst is necessary to study its activity for the soot combustion. This addition was done by immersing the Co,Ba,K/ZrO<sub>2</sub>-foam into a soot suspension either in water or *n*-hexane. When the former was used as solvent, the soot conglomerates were quite large and a non-uniform distribution along the structured catalyst surface was observed (Fig. 9c and d), indicating that water is inappropriate to disperse soot particles to evaluate the catalytic properties of the produced coating. Moreover, water can dissolve some of the active components of the coating during the immersion process, such as KNO<sub>3</sub>, modifying the original composition of the catalyst. On the other hand, when the solvent was *n*-hexane, a good distribution of small soot agglomerates on the catalytic surface was obtained (Fig. 9a and b), which produced a better soot–coating contact with good reproducibility. These characteristics (formation of small soot agglomerates homogeneously distributed all over the coating) are important in order to analyze the activity and stability of the obtained coatings.

In order to examine the influence of the soot–coating contact on the temperature at which the combustion rate is maximal, three soot suspensions of different concentration (600, 1500 and 6000 ppm) were used for soot impregnation. The calculated coating–soot ratios were 6, 4, and 2, respectively. As it is expected, the higher the soot concentration (coating–soot ratio: 2), the worse the soot–coating contact, since as the catalytic coating is entirely covered with soot particles, the incorporation of additional particles takes place over the previously deposited layer of soot. Consequently, an important non-catalytic oxidation of soot occurs and the temperature of maximum combustion of soot increases, as it is observed in the temperature program oxidation profiles for the soot/structured catalyst (Co,Ba,K/ZrO<sub>2</sub>-foam) and for the soot/structured support (ZrO<sub>2</sub>-foam) (Fig. 10).

Even though the coating microanalysis using SEM-EDX determined that the active component distribution was not homogeneous (Tables 2 and 3), the repetitivity of the TPO profiles (Fig. 11) is remarkable, suggesting that the influence of this non-uniform element concentration between flake and crack regions over the catalytic activity is not significant. The total carbon amount of the TPO peaks differ less than 15% among those of the structured catalyst and 10% among those corresponding to the structured support. Comparing the average total carbon amount between samples, structured catalyst and support, there is a difference owing to the different sample sizes (Fig. 11). Nevertheless, the similarity between the catalyst areas and those corresponding to the support indicates repetitivity in the loading of soot since the experiments have been carried out over either one piece of the structured catalyst or one piece of the structured support (repeatedly loading soot and burning it, loading soot again and burning it again).

Catalysts were evaluated adding NO to the feed because NO is usually present in diesel exhausts. As it is known, the higher oxidation power of NO<sub>2</sub> (formed by the reaction between NO and O<sub>2</sub>) reduces the temperature of maximum combustion rate (Fig. 12). The similarity of temperatures of maximum combustion rate when feeding NO also suggests the stability of the structured catalyst. In addition, the TPO of the coating–soot ratios: 6 and 4 have the CO<sub>2</sub> concentration maximum temperatures around 370 °C (Fig. 12), suggesting that even though the amount of soot

for the low coating–soot ratio was higher, their catalyst–soot contacts were comparable. Moreover, the carbon conversion profiles for both ratios were similar and shifted to low temperatures compared with that of ratio: 2 (Fig. 13).

The comparison of carbon conversion between powder and structured catalysts shown in Fig. 14 indicates that at lower conversions, the catalytic behavior presents the same trend. However, for carbon conversions higher than 5%, the curve of the structured catalyst shifts to higher temperatures. In a previous work, the powder Co,Ba,K/ZrO<sub>2</sub> catalyst was studied as a catalyst for soot combustion [29]. Varying the catalyst–soot ratios and the NO contents in the feed, the NO reaction order and the global activation energy of the reaction were estimated, being 0.5 and 20 kcal/mol respectively. To obtain these values, data at low carbon conversions were used. Therefore, this activation energy and this NO reaction order could also be valid for the structured catalyst.

As previously mentioned, the structured catalyst curve shifted to higher temperatures at carbon conversions above 5% (Fig. 14). This performance is expected since coating–soot contact is close to become a loose one [38] whereas the powder catalyst–soot mixture was prepared in an agate mortar during 3 min so as to obtain a tight contact.

## 5. Conclusions

Cobalt, barium and potassium deposited on ZrO<sub>2</sub> (Co,Ba,K/ZrO<sub>2</sub>), previously tested as a good powder catalyst for the combustion of soot [29], have been effectively coated on an Al<sub>2</sub>O<sub>3</sub> foam by a sequential procedure. After obtaining a layer of ZrO<sub>2</sub> by washcoating, the active components were incorporated by impregnation. The ZrO<sub>2</sub> layer increased the surface area of the structure and avoided the interaction among active elements and alumina surface.

The observed cracking of the coating was produced due to both the shrinkage of the Zr(OH)<sub>x</sub> film during the drying process and the high temperature treatment needed to remove and burn the acetic acid present as colloidal suspension stabilizer. Although the film morphology presented an interconnected crack structure, the ZrO<sub>2</sub> layer had good adhesion. Interestingly, the stability of the final coating increased after the impregnation of the active components (K, Ba and Co) probably due to a partial melting of the potassium salt.

Soot particles were incorporated to the structured catalyst using a slurry in hexane, thus giving place to a loose contact between soot and the catalyst, in agreement with van Setten et al. [38]. Despite the non-homogeneous nature of the foam, the application of the said method yielded satisfactory results regarding the repetitiveness of the catalytic behavior.

Although a shrinkage–crack pattern of flakes (mainly composed of Co,Ba,K/ZrO<sub>2</sub>) and cracks (rich in Al<sub>2</sub>O<sub>3</sub>) was observed in the catalytic film, the system showed to be active and stable for the catalytic combustion of soot. The maximum in the combustion rate depended upon the amount of soot loaded and the presence of NO in the feed, having a performance comparable to that obtained with the powder catalyst.

## Acknowledgments

The authors wish to acknowledge the financial support received from ANPCyT, CONICET and UNL. Thanks are also given to Elsa Grimaldi for the English language editing.

## References

- [1] B.A.A.L. van Setten, J.M. Schouten, M. Makkee, J.A. Moulijn, *Appl. Catal. B: Environ.* 28 (2000) 253–257.
- [2] J.P.A. Neeft, M. Makkee, J.A. Moulijn, *Fuel Process. Technol.* 47 (1996) 1–69.
- [3] B.A.A.L. van Setten, M. Makkee, J.A. Moulijn, *Catal. Rev. Sci. Eng.* 43 (4) (2001) 489–564.
- [4] M.A. Gómez-García, V. Pitchon, A. Kiennemann, *Environ. Int.* 31 (2005) 445–467.
- [5] B.R. Stanmore, V. Tschamber, J.-F. Brillhac, *Fuel* 87 (2008) 131–146.
- [6] D. Fino, *Sci. Tech. Adv. Mater.* 8 (2007) 93–100.
- [7] M.V. Twigg, *Appl. Catal. B: Environ.* 70 (2007) 2–15.
- [8] V.G. Milt, M.A. Ulla, E.E. Miró, in: A. Gil, S.A. Korili (Eds.), *Recent Research Developments in Environmental Technology*, Transworld Research Network, 2008, pp. 57–78.
- [9] M. Ambrogio, G. Saracco, V. Specchia, *Chem. Eng. Sci.* 56 (2001) 1613–1621.
- [10] M.V. Twigg, J.T. Richardson, *Trans. I. Chem. E* 80 (A) (2002) 183–189.
- [11] J.T. Richardson, M. Garrat, J.-K. Hung, *Appl. Catal. A: Gen.* 255 (2003) 69–82.
- [12] P. Ciambelli, V. Palma, P. Russo, S. Vaccaro, *Cat. Today* 75 (2002) 471–478.
- [13] A. Setiabudi, M. Makkee, J.A. Moulijn, *Appl. Catal. B: Environ.* 42 (2003) 35–45.
- [14] P. Ciambelli, V. Palma, P. Russo, S. Vaccaro, *Cat. Today* 73 (2002) 363–370.
- [15] B.A.A.L. van Setten, C.G.M. Spitters, J. Bremmer, A.M.M. Mulders, M. Makkee, J.A. Moulijn, *Appl. Catal. B: Environ.* 42 (2003) 337–347.
- [16] P. Ciambelli, G. Matarazzo, V. Palma, P. Russo, E. Merlone Borla, M.F. Pidria, *Topics Catal.* 42–43 (2007) 287–291.
- [17] P. Ciambelli, V. Palma, P. Russo, S. Vaccaro, *Chem. Eng. Sci.* 60 (2005) 1619–1627.
- [18] N.K. Labhsetwar, R.B. Biniwale, R. Kumar, M.A. Bawase, S.S. Rayalu, T. Mitsushashi, H. Haneda, *Curr. Sci.* 87 (2004) 1700–1704.
- [19] A. Setiabudi, M. Makkee, J.A. Moulijn, *Topics Catal.* 30–31 (2004) 305–310.
- [20] V. Palma, P. Russo, M. D'Amore, P. Ciambelli, *Topics Catal.* 30–31 (2004) 261–266.
- [21] D. Fino, P. Fino, G. Saracco, V. Specchia, *Chem. Eng. Sci.* 58 (2003) 951–958.
- [22] P. Russo, P. Ciambelli, V. Palma, S. Vaccaro, *Topics Catal.* 22 (2003) 123–129.
- [23] P. Ciambelli, V. Palma, P. Russo, M. D'Amore, *Stud. Surf. Sci. Catal.* 145 (2002) 367–370.
- [24] V. Palma, M. D'Amore, P. Russo, A. D'Arco, P. Ciambelli, *Comb. Sci. Tech.* 174 (2002) 295–308.
- [25] M. Ambrogio, G. Saccaro, V. Specchia, G. van Coen, M. Makkee, J.A. Moulijn, *Separ. Purif. Tech.* 27 (2002) 195–209.
- [26] M.A. Peralta, V.G. Milt, L.M. Cornaglia, C.A. Querini, *J. Catal.* 242 (2006) 118–130.
- [27] S. Biamino, P. Fino, D. Fino, N. Russo, C. Badini, *Appl. Catal. B: Environ.* 61 (2005) 322–330.
- [28] V.G. Milt, C.A. Querini, E.E. Miró, M.A. Ulla, *J. Catal.* 220 (2003) 424–432.
- [29] V.G. Milt, E.D. Banús, M.A. Ulla, E.E. Miró, *Cat. Today* 133–135 (2008) 435–440.
- [30] V.G. Milt, M.L. Pissarello, E.E. Miró, C.A. Querini, *Appl. Catal. B: Environ.* 41 (2003), 397–411.
- [31] P.G. Harrison, I.K. Ball, W. Daniell, P. Lukinskas, M. Céspedes, E.E. Miró, M.A. Ulla, *Chem. Eng. J.* 95 (2003) 47–55.
- [32] S. Chang, R. Doong, *Chem. Mater.* 17 (2005) 4837–4844.
- [33] F.A. Miller, in: D.W. Mayo, F.A. Miller, R.W. Hannah (Eds.), *Course notes on the interpretation of infrared and Raman spectra*, Wiley-Interscience, Hoboken, New Jersey, 2003, pp. 297–354.
- [34] W. Lan, X. Wang, P. Xiao, *J. Eur. Ceram. Soc.* 26 (2006) 3599–3606.
- [35] M. Valentini, G. Groppi, C. Cristiani, M. Levi, E. Tronconi, P. Forzatti, *Catal. Today* 69 (2001) 307–314.
- [36] A.E.W. Beers, T.A. Nijhuis, F. Kapteijn, J.A. Moulijn, *Microporous Mesoporous Mater.* 48 (2001) 279284.
- [37] J.M. Zamaro, M.A. Ulla, E.E. Miró, *Chem. Eng. J.* 106 (2005) 25–33.
- [38] B.A.A.L. van Setten, J. Bremmer, S.J. Jelles, M. Makkee, J.A. Moulijn, *Cat. Today* 53 (1999) 613–621.
- [39] M.S. Gross, M.A. Ulla, C.A. Querini, *Appl. Catal. A: Gen.* 360 (2009) 81–88.
- [40] L.M. Martínez, E.D.M. Frías, M.A. Centeno, A. Paúl, M. Montes, J.A. Odriozola, *Chem. Eng. J.* 136 (2008) 390–397.
- [41] M. Wegmann, B. Michen, T. Luxbacher, J. Fritsch, T. Graule, *Water Res.* 42 (2008) 1726–1734.
- [42] R.S. Patil, M.D. Uplane, P.S. Patil, *Appl. Surf. Sci.* 252 (2006) 8050–8056.
- [43] X. Gu, P.A. Trusty, E.G. Butler, C.B. Ponton, *J. Eur. Ceram. Soc.* 20 (2000) 675–684.